Stability of Externally Driven Magnetic Islands in a Helical Plasma*⁾

Seiya NISHIMURA, Shinichiro TODA, Masatoshi YAGI[1,2] and Yoshiro NARUSHIMA

National Institute for Fusion Science, Toki 509-5292, Japan
[1]*Japan Atomic Energy Agency, Rokkasho-mura, Kamikita-gun, Aomori 039-3212, Japan*
[2]*Research Institute of Applied Mechanics, Kasuga 816-8580, Japan*

Influence of external resonant magnetic perturbation (RMP) on a helical plasma is numerically investigated, using a set of reduced magnetohydrodynamic equations. Coexistence of the resistive interchange mode and RMP is simulated. In nonlinear simulations, saturated magnetic islands by the RMP typically show two states: oscillating small islands and locked large islands. In the former state, rotation of magnetic islands by neoclassical transport-driven poloidal flows disturbs growth of islands. On the other hand, in the latter state, locking of poloidal flows due to the RMP and growth of islands occur simultaneously. It is found that the curvature driven current enhances magnetic reconnection, and width of the large islands overcomes that of vacuum islands.

1. Introduction

Externally imposed resonant magnetic perturbation (RMP) by a set of external current coils or error fields is of great interest in magnetic fusion plasmas. In helical devices, such as the Large Helical Device (LHD) and the TJ-II, the RMP produces magnetic islands in the vacuum magnetic field (vacuum islands), and plasma response modifies island state. As an extreme example of the plasma response, bifurcation of equilibria between with and without islands has been observed in the helical devices, where spontaneous shrink of islands is called 'self-healing' [1].

Numerical simulations using reduced fluid equations have been developed to investigate influence of the RMP on helical plasmas. It is pointed out that size of the islands is affected by the resistive interchange mode [2, 3] and/or island-driven poloidal flows [4]. However, influence of neoclassical transport has not been discussed so far. In our previous study, using a theoretical model, it is shown that the self-healing of islands is clearly reproduced, when the neoclassical transport-driven poloidal flows is taken into account [5]. In this paper, we report that such mechanism is actually observed in reduced fluid simulations.

2. Model Equation

We introduce a conventional set of reduced magnetohydrodynamic (MHD) equations, that model torus plasmas with large aspect ratios by cylindrical plasmas including additional three-dimensional effects. In our previous

work, the similar model is used to simulate the interaction between the resistive ballooning mode with the RMP in tokamak plasmas [6]. Because of difficulties in multi-scale simulations with parallel thermal transport, ion and electron temperatures are assumed to be constant and equal to each other. In addition, we neglect electron and ion diamagnetic drifts and electron inertia for simplicity. The diamagnetic drifts which are the same order as the neoclassical flows might modify our results. The vorticity equation, the Ohm's law, the continuity equation, and the equation of parallel ion motion are given respectively by

$$\frac{\mathrm{d}}{\mathrm{d}t}\nabla_\perp^2\phi = \nabla_\parallel j_\parallel + [\Omega, p] + \mu\nabla_\perp^4\phi, \tag{1}$$

$$\frac{\partial A}{\partial t} = -\nabla_\parallel\phi + \eta_\parallel\left(j_\parallel - j_{\parallel 0}\right), \tag{2}$$

$$\frac{\mathrm{d}p}{\mathrm{d}t} = \hat\beta\left([\Omega, \phi] - \nabla_\parallel v_\parallel + \eta_\perp\nabla_\perp^2 p\right), \tag{3}$$

$$\frac{\mathrm{d}v_\parallel}{\mathrm{d}t} = -\nabla_\parallel p + \mu_\parallel\nabla_\perp^2 v_\parallel, \tag{4}$$

with $j_\parallel = -\nabla_\perp^2 A$, $\mathrm{d}/\mathrm{d}t = \partial/\partial t + [\phi, \ ]$, $\nabla_\parallel = \partial/\partial z - [A, \ ]$ and $\nabla_\perp = \hat{r}(\partial/\partial r) + \hat{\theta}(1/r)(\partial/\partial\theta)$, where the bracket is defined by $[f, g] = \hat{z}\cdot\nabla f\times\nabla g$ for arbitrary variables f and g. The cylindrical coordinate variables (r, θ, z) correspond to the minor radial length, the poloidal phase angle, and the toroidal length in the torus coordinate, respectively, and $(\hat{r}, \hat{\theta}, \hat{z})$ are unit vectors. The time and lengths are normalized as $t/\tau_A \to t$, $r/a \to r$, $z/R_0 \to z$, with $\tau_A = R_0/v_A$, where v_A is the Alfvén velocity, a is the minor radius, and R_0 is the major radius of the torus. The variables $\{\phi, A, p, v_\parallel\}$ denote the normalized electrostatic potential, vector potential parallel to the ambient magnetic

field, electron pressure and plasma velocity parallel to the ambient magnetic field, respectively. β is the ratio between the kinetic pressure and the magnetic pressure at the plasma center and $\hat{\beta} = \beta/(1 + \beta)$. The transport coefficients $\{\mu_\perp, \mu_\parallel, \eta_\parallel, \eta_\perp\}$ denote the perpendicular viscosity, the parallel viscosity, the parallel resistivity and the perpendicular resistivity, respectively, where those coefficients are assumed to include both classical transport and anomalous effects due to microscopic turbulence. The detailed modeling of the anomalous effects is still an open issue [7]. Using the averaging method [8], Ω gives the normalized average magnetic field line curvature of helical plasmas such that $\partial\Omega/\partial r = (\epsilon N/l)(4r\iota + r^2\iota')$, where $\epsilon = a/R_0$, $2\pi\iota$ is the rotational transform and $\{l, N\}$ are the pole and pitch numbers of helical winding, respectively. We neglect the toroidal curvature for simplicity. The arbitrary variable $f = f(r, \theta, z, t)$ is expanded as $f_0(r) + \sum_{m,n} \tilde{f}_{m,n}(r, t) \exp\{i(m\theta - nz)\}$, where m is the poloidal mode number and n is the toroidal mode number. The boundary conditions for the perturbation amplitudes are basically given such that $\tilde{f}_{m,n}(0, t) = \tilde{f}_{m,n}(1, t) = 0$ for $(m, n) \neq (0, 0)$ and $\tilde{f}_{0,0}(0, t) = (\partial\tilde{f}_{0,0}/\partial r)|_{r=1} = 0$. To introduce the RMP, an edge boundary condition is imposed on the vector potential such that $\tilde{A}_{m',n'}(1, t) = \psi_a$, where (m', n') are the poloidal and toroidal mode numbers of the RMP, respectively. The detail of the modeling of the RMP is described in Ref. [6]. Radial integral of the $(0, 0)$ component of Eq. (1) gives an evolution equation of poloidal flows such that

$$\frac{\partial v_\theta}{\partial t} = \frac{1}{r}\int r\left[\phi, \nabla_\perp^2\phi\right]_{0,0}\mathrm{d}r + \frac{1}{r}\int r\left[A, j_\parallel\right]_{0,0}\mathrm{d}r$$
$$+ \mu\frac{\partial}{\partial r}\left[\frac{1}{r}\frac{\partial}{\partial r}(rv_\theta)\right] + \nu^{\mathrm{nc}}(V_0 - v_\theta), \qquad (5)$$

where $v_\theta = \partial\tilde{\phi}_{0,0}/\partial r$ is the poloidal flow velocity, ν^{nc} is the normalized ion neoclassical damping rate, $V_0 = -2\delta(\mathrm{d}p_0/\mathrm{d}r)$ is the normalized ion neoclassical flow velocity where δ is the normalized ion skin depth and the subscript $0, 0$ indicates a summation of $(0, 0)$ components. In addition, the neoclassical viscosity might be well approximated by that without RMP when the toroidal magnetic field ripple produced by magnetic islands are much smaller than that by the main helical coils. In Eq. (5), the electron neoclassical viscosity is neglected, where such simplification is reasonable when ion and electron temperatures are equal to each other. Considering Eq. (5), a source term is implemented in the right-hand side of Eq. (1) for the $(0, 0)$ mode such that $\nu^{\mathrm{nc}}[(1/r)\partial_r(rV_0) - \nabla_\perp^2\tilde{\phi}_{0,0}]$. In the simulations, default parameters are chosen such that $\beta = 0.01$, $\delta = 10^{-2}$, $\epsilon = 0.2$, $\mu = 10^{-5}$, $\eta_\parallel = 10^{-5}$, $\hat{\beta}\eta_\perp = 10^{-5}$, $\mu_\parallel = 10^{-5}$, $(m', n') = (2, 1)$, $\psi_a = 5 \times 10^{-4}$, $(l, N) = (2, 10)$. The initial profiles are given by $\iota = 0.4 + 1.2r^4$, $p_0 = (\beta/\epsilon)(1 - r^2)$, $v_{\parallel 0} = 0$ and $j_{\parallel 0} = \mathrm{d}(r^2\iota)/\mathrm{d}r$, and ϕ_0 is specified in the following sections. For the initial profile, resonant modes satisfy $5/8 \leq m/n \leq 5/2$, and the $m/n = 2$ rational surface is located at $r = 0.54$. Fourier modes with $-20 \leq m \leq 20$
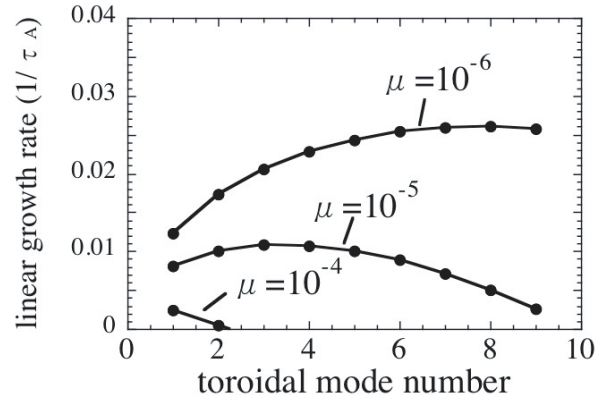

Fig. 1 Toroidal mode number dependence of linear growth rate of the resistive interchange mode with $m/n = 2$. Three cases with different values of the perpendicular viscosity are plotted.

and $-10 \leq n \leq 10$ are solved in the simulations. Note that our model is not applicable to modes with $n > N = 10$, because of the averaging method.

3. Linear Stability

Firstly, we numerically solve the linearized Eqs. (1)-(4), where ϕ_0 is set to satisfy $\partial\phi_0/\partial r = V_0$. Using the default parameters, the linear interchange mode is unstable for many resonant modes in the core region where the magnetic shear ($\propto \mathrm{d}\iota/\mathrm{d}r$) is small. On the other hand, the modes are stable in the outer region, because of the large magnetic shear. In addition, it is observed that some nonresonant modes with $5/2 < m/n$ are also weakly unstable.

Here, we focus on resonant modes with $m/n = 2$, since the RMP is imposed at the $m/n = 2$ surface. Figure 1 shows the linear growth rate of the resistive interchange mode with $m/n = 2$. Using the default value of the perpendicular viscosity, $\mu = 10^{-5}$, the growth rate has a peak at $n = 3$. In Fig.1, the cases with $\mu = 10^{-6}$ and $\mu = 10^{-4}$ are also plotted, and it is found that the increase of μ tends to stabilize the mode. Similarly, we confirmed that the increase of $\mu_\parallel$ and $\hat{\beta}\eta_\perp$ stabilize the mode, on the other hand, the mode is destabilized when $\eta_\parallel$ and β are increased. In addition, the mode stability is not sensitive to the value of δ, i.e., the magnitude of the ion neoclassical flow velocity.

It is necessary to mention that eigenfunction of the $(m, n) = (2, 1)$ does not have purely odd or even parity around the rational surface. For example, we expect $\tilde{A}_{2,1}$ is an odd function in the slab geometry, but there exists even component in the cylindrical geometry [2]. As a result, growth of the $(2, 1)$ interchange mode produces magnetic islands in the nonlinear phase, as shown in the next section.

4. Nonlinear Simulation

In the next step, the nonlinear Eqs. (1)-(4) are numerically solved with the default parameters, where we set $\phi_0 = 0$. Poloidal flows are driven by the ion neoclassical
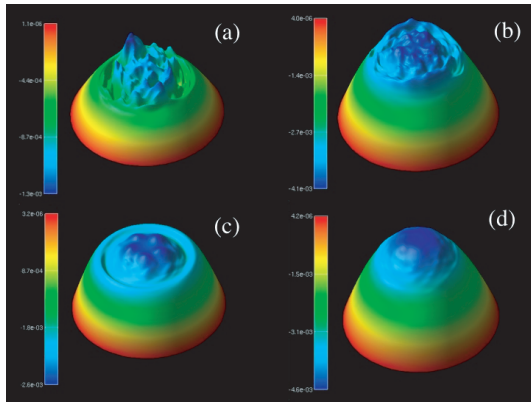
Fig. 2 Bird's-eye views of the electrostatic potential at an early stage ($t = 300$) for (a) $v^{nc} = 10^{-3}$ and (b) $v^{nc} = 10^{-2}$, and those at a nonlinearly saturated stage ($t = 2000$) for (c) $v^{nc} = 10^{-3}$ and (d) $v^{nc} = 10^{-2}$.

Fig. 3 Radial profile of poloidal flow source (dashed line) and nonlinearly saturated poloidal flows ($t = 5000$) for $v^{nc} = 10^{-3}$ and $v^{nc} = 10^{-2}$ (solid lines). The bars with arrows indicate magnetic island region for each case.

Fig. 4 Contour plots of the nonlinearly saturated helical flux function ($t = 5000$) for (a) $v^{nc} = 10^{-3}$ and (b) $v^{nc} = 10^{-2}$.

Fig. 5 v^{nc} dependence magnetic island width in the nonlinearly saturated stage.

drag force as shown in Eq. (5), and $\tilde{\phi}_{0,0}$ is expected to have parabolic profile in the absence of other force. To avoid a numerical problem at the core region, the poloidal flow source is set to zero in the range of $0 \leq r \leq 0.1$. Nonlinear simulations with different values of v^{nc} are shown in the following part.

Figure 2 shows time evolution of the electrostatic potential, Re $\sum_{m,n} \tilde{\phi}_{m,n} \exp(im\theta)$ for two cases with $v^{nc} = 10^{-3}$ and $v^{nc} = 10^{-2}$. At an early stage (Figs. 2 (a) and (b)), the excitation of the resistive interchange mode is observed near the core region. In the nonlinear growing stage, unstable modes collapse the pressure profile, where the convective heat transport by the $(m, n) = (2, 5)$ mode plays a dominant role, and the pressure becomes flat near the core region. For this reason, the interchange mode loses most of the instability source, then saturates at low level. It is clearly observed that structure of the electrostatic potential in the nonlinearly saturated stage depends on the value of v^{nc}. Concentric structure is formed around the $m/n = 2$ surface for the small v^{nc} case (Fig. 2 (c)), but such structure does not appear for the large v^{nc} case (Fig.2 (d)).

Figure 3 shows the nonlinearly saturated radial profile of poloidal flows and magnetic island region for the cases with $v^{nc} = 10^{-3}$ and $v^{nc} = 10^{-2}$. It is found that poloidal flows are damped near the central axes of magnetic islands close to the $m/n = 2$ surface, when large islands are excited. The damping of poloidal flows indicates that the rotation of large islands is locked. The concentric structure of the electrostatic potential shown in Fig. 1 (c) corresponds to the damping of poloidal flows in Fig. 3. On the other hand, poloidal flows are not strongly affected when islands are small and rotating. To check the structure of magnetic surface, we introduce a normalized helical flux function defined by $h_{2,1} = (r(d\iota/dr))|_{r_s}(r-r_s)^2/2 + \text{Re}[\tilde{A}_{2,1} \exp(i2\theta)]$, where $\nabla h_{2,1}$ is perpendicular to the magnetic field lines perturbed by the $(2, 1)$ mode at $z = 0$. Note that the helical flux function maps only the magnetic field perturbation by
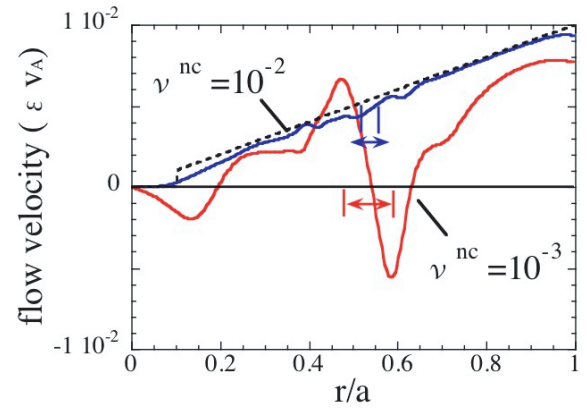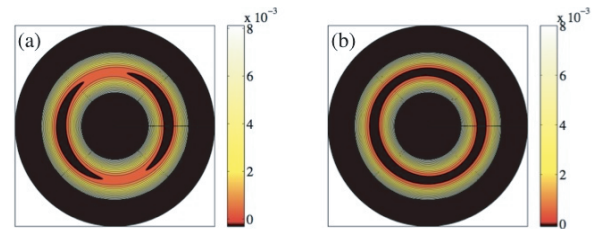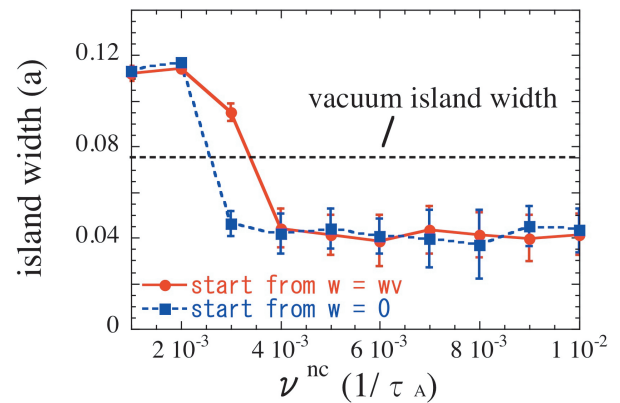
magnetic islands. Figure 4 shows contour plots of the helical flux function, where magnetic island structure is identified in the case with (a) $v^{nc} = 10^{-3}$, whereas that is not clearly distinguished in the case with (b) $v^{nc} = 10^{-2}$.

Figure 5 shows v^{nc} dependence of the nonlinearly saturated magnetic island width, where we fix $\tilde{A}_{2,1}(r = 1) = \psi_a$. Two initial conditions are examined: simulations started from the vacuum field limit $w = w_v$ ($\tilde{A}_{2,1}(r) = \psi_a r^2$ for $0 \leq r < 1$) and those started from the no island limit $w = 0$ ($\tilde{A}_{2,1}(r) = 0$ for $0 \leq r < 1$). In Fig. 5, the 'vac-

uum island width' is defined by $w_v = 4\sqrt{\psi_a r_s^{m'}/(d\iota/dr)|_{r_s}}$, the island width is $w = 4\sqrt{\tilde{A}_{2,1}|_{r_s}/(d\iota/dr)|_{r_s}}$. It is found that the saturated island width drastically changes around $\nu^{nc} = 3 \times 10^{-3}$. Moreover, hysteresis nature is observed around $\nu^{nc} = 3 \times 10^{-3}$. It is remarkable that large magnetic island width in the low ν^{nc} regime is larger than that of vacuum islands.

Cases without the average magnetic field line curvature are also simulated and the increase of the magnetic island width is found to be due to the curvature effect. Moreover, it is found that the shrink threshold of magnetic islands is affected by the curvature effect. The curvature driven current estimated by the ideal MHD equilibrium, $\nabla_\parallel j_\parallel + [\Omega, p] = 0$ and $\nabla_\parallel p = 0$, is the (resonant) perturbed Pfirsch-Schlüter current, which drives the curvature driven tearing mode. In addition, the curvature driven current might be affected by non ideal effects. Based on the analytical theory [5], the shrink threshold of islands in the absence of the curvature effect is estimated as $\nu_{nc} = 1.8 \times 10^{-4}$, where the balance between the neoclassical force and the Lorentz force is essential in our parameters. This estimation is consistent with the simulations without the curvature effect.

5. Summary

Linear stability analysis of the resistive interchange mode and nonlinear simulations of the mode with resonant magnetic perturbation (RMP) are investigated using a reduced magnetohydrodynamic equations for a helical plasma. In nonlinear simulations, it is confirmed that neoclassical transport-driven poloidal flows work as damping mechanism of magnetic islands by the RMP.

Acnowledgements

[1] Y. Narushima *et al.*, Nucl. Fusion **51**, 083030 (2011).
[2] K. Saito *et al.*, Phys. Plasmas **17**, 062504 (2010).
[3] T. Unemura *et al.*, Phys. Plasmas **11**, 1545 (2004).
[4] L. Garcia *et al.*, Nucl. Fusion **43**, 553 (2003).
[5] S. Nishimura *et al.*, Plasma Fusion Res. **5**, 040 (2011).
[6] S. Nishimura and M. Yagi, Plasma Fusion Res. **6**, 2403119 (2011).
[7] A. Ishizawa and N. Nakajima, Phys. Plasmas **17**, 072308 (2010).
[8] H.R. Strauss, Plasma Physics **22**, 733 (1980).